Detectability of Quantum Effects in Gravitational Waves Emitted by Binary Black Hole Mergers

LIGO SURF 2020: Interim Report 2

Zoë Haggard
Pomona College

Mentors: Alan J. Weinstein and Colm Talbot
LIGO Collaboration, Caltech

(Dated: July 31, 2020)

Gravitational wave detectors such as Advanced LIGO and Advanced Virgo provide a test of the theory of general relativity in the strong-field, highly dynamical regime, such as in compact binary coalescences. General relativity, a purely classical theory, does not incorporate quantum mechanics. It is thought, however, that quantum mechanics must modify gravity; quantum uncertainty must manifest itself during the merger of two black hole horizons. These quantum mechanical effects could be observable in gravitational waves detected by LIGO as small perturbations in the signal waveform and higher harmonics, not explainable by classical general relativity. We propose to study the *phenomenology* and *detectability* of such quantum mechanical effects from binary black hole mergers for future LIGO observations.

I. MOTIVATION

In his general theory of relativity (GR), Einstein predicts the existence of gravitational waves. Just as an accelerating charge produces electromagnetic radiation, an accelerating mass will create gravitational radiation, or, gravitational waves (GWs). GWs emit outwards at the speed of light, and, in the far-field, are described by a complex strain, $h = h_+ - ih_\times$, on space-time: the passing waves cause the distance between freely falling objects ('test masses') to oscillate at the frequency and amplitude of the GWs [1]. But gravitation, compared to electromagnetism, is much weaker. To observe gravitational radiation on Earth, highly massive and dynamic systems – such as coalescing compact binary black hole (BBH) systems – are needed in conjunction with large and precise detectors. In recent years, the Laser Interferometer Gravitational-Wave Observatory (LIGO) and Advanced Virgo have successfully observed GWs from compact binary mergers [2, 3].

The coalescence of a BBH system is defined by three major phases: inspiral, merger, and ringdown [4]. In the inspiral, the two black holes emit gravitational waves (roughly) proportional to their orbital frequencies; their orbital radius decreases with the GW emission. After the last stable orbit, the two horizons plunge into each other and merge during the merger phase. Finally, once the BHs' horizons come together, the system falls to equilibrium in the ringdown by emitting GWs at specific modes, called quasi-normal modes (QNMs). The frequency and damping time of these modes can be calculated from black hole perturbation theory, which takes into account the final black hole's spin and mass; amplitude and phase of the modes, however, depend on the characteristics of the merger [5].

Analytically representing these modes is a challenge and many methods have be used to numerically (or semi-analytically) calculate QNMs [6]. For GW observations, the loudest QNM tends to be the (2, 2) mode. The complex angular frequency of the fundamental (2, 2) mode for a gravitationally perturbed Schwarzschild BH is,

$$\omega_n = \frac{0.7474c}{R_s} - i\frac{0.178c}{Rs} \tag{1}$$

where c is the speed of light, and R_s is the Schwarzschild radius, $2GM/c^2$ [5]. As an example, a BH with $10M_\odot$ will have a frequency ($\Re(\omega)/2\pi$) of 1203 Hz and a damping time ($1/\Im(\omega)$) of 0.34 ms.

Generally, the ringdown strain at a GW-detector is a linear superposition of damped sinusoids,

$$h(t) = \sum_{j=1} A_j e^{2i\pi f_{0,j} t + i\phi_j} e^{-\frac{t}{\tau_j}} \tag{2}$$

where A_j is the amplitude of term j, $f_{0,j}$ is the central frequency of the particular mode, ϕ_j is the phase shift, and τ_j is the decay time, or the time required for the amplitude to drop by a factor of $1/e$ [7]. Referring back to Equation 1 for a Schwarzschild BH (2, 2 mode, $f_{0,1} = 2\pi\Re(\omega_1)$ and $1/\tau_1 = \Im(\omega_1)$.

The Fourier transform, which shifts to the frequency domain, is a useful tool for signal analysis: it helps to pinpoint higher harmonics and easily analyze the other wave characteristics. The Fourier transform of a damped sinusoid is the Lorentzian [8]. Centered at f_0, the Lorentzian is written as,

$$\tilde{h}(f) = \sum_{j=1} A_j e^{i\phi_j} \frac{1}{2\pi} \frac{\gamma_j}{((f_j - f_{0,j})^2 + \frac{1}{2}{\gamma_j}^2)} \tag{3}$$

where $f_{o,j}$ is the frequency of the mode and $\gamma_j = \frac{1}{\tau_j}$.

The signals received at detectors are found to be dominantly quadrupolar, as predicted by GR [4]. Therefore,

for waveform creation, the gravitational radiation is assume just the (2, 2) mode for ease of analysis. This is usually a good assumption, as higher order modes – modes with $l > 2$ and $m \neq 2$ – tend to be negligible. These higher modes have magnitudes are much smaller than the dominant quadrupole, making them hard to disentangle from the noise. With just the dominant mode, intrinsic characteristics, such as the individual BH's mass and spin, and extrinsic characteristics, such as location, inclination (relative to the observer's line of sight), and the time of merger, can be inferred from the strain received at a network of detectors [9].

Recently, however, higher harmonics have been observed in compact binary mergers. GW190412 and GW190814, for instance, both show evidence of an octopole (3, 3) mode [7, 10]. This opens up a new domain for testing more finely the predictions of GR. As of yet, there have been no inconsistencies found, but the study of higher order modes – black hole spectroscopy – presents a way to uncover inconsistencies in GR.

Deviations from GR are expected. For instance, there is no unified theory of gravity and quantum mechanics; GR and quantum mechanics, among other things, disagree about what happens past the event horizon of a BH. In the classical GR picture, the inside of a BH is empty except for the infinitely dense region of the singularity. But, according to quantum mechanics, quantum uncertainty should become important on Planck scales; meaning, near the singularity, space is not empty, but full of quantum fluctuations of matter fields [11].

One way to get around this conundrum is to explore what would happen if a black hole was in fact a BH-imitator, or an exotic compact object (ECO). ECOs, which are included in various theories of quantum gravity around BHs, allow for the union of GR and quantum mechanics. An ECO is *not* empty, but is rather made up of some form of exotic matter. There, however, are very few concrete predictions of the observable differences these ECOs would produce.

Recent work done by Brustein *et al*, which incorporates a collapsed polymer model ECO, finds differences in the quasi-normal ringdown spectrum [12, 13]. The collapsed polymer models the BH as a Schwarzschild-radius sized soup of interacting, closed strings. As a more general approach, the stringy matter can be treated as a fluid with an index of refraction, n_{ref}, where n_{ref} is defined as v_{sound}/c. Matching the boundary conditions between inside and outside the polymer, it is found that relativistic modes ($v_{sound} \lesssim c$) are suppressed, while sub-relativistic modes ($v_{sound} < c$) are able to leak past the horizon. In other words, n_{ref} must be greater than 1 [13].

The index of refraction can also be related to the properties of the matter. In the stringy polymer case, n_{ref} inversely depends on the likelihood of string interaction, g_s, or the quantum string coupling; this a number between 0 and 1. In the GR limit, g_s is 0, implying zero interaction between stringy matter, and thus an infinite n_{ref}; in other words, no modes can leak past the horizon. A large g_s, on the other hand, implies many interactions between strings [14]. A g_s close to 1 is nonphysical, however, as an analysis of GW150914 and GW151226 suggest that g_s^2, using this model, is (roughly) less than 0.65 [13]. This translates to an n_{ref} of at *least* 1.25.

In summary, as the BH-copycat horizon is deformed during the ringdown, the stringy fluid creates additional fluid modes that are quantum in nature. These modes have specific complex angular frequencies in *addition* to the regular GR modes. In the limit of $n_{ref} > 1$ – sub-relativistic modes – these angular frequencies can be written as,

$$\omega_p = \frac{pc\pi}{2R_s n_{ref}} - i\frac{c}{R_s n_{ref}^2} \tag{4}$$

where p is an odd integer, c is the speed of light, R_s is equivalent to the r_+ Kerr solution, and n_{ref} is the refractive index of the matter. If we compare the $p = 1$ mode to the gravitationally perturbed Schwarzschild (2, 2) mode (Equation 1), given that n_{ref} must be greater than 1, we see that the fluid mode has a lower frequency (by around a factor of $1/n_{ref}$) and a longer damping time (by around a factor of $6n_{ref}^2$).

In the time domain, these additional ringdown modes have the same form as Equation 2, but are composed of different frequencies, amplitudes, and damping times [13]. These modes are also slightly delayed relative to the GR modes, with a delay time (t_s) that is proportional to $1/\Re\omega$, or by around a factor of $1/n_{ref}$.

Putting the quantum ringdown in terms of GR QNM (Equation 2), the new modes can be written as,

$$h(t) = \sum_{j=1}\sum_{p=1}(A_j\frac{A_{q,p}}{A_j})e^{i(t-t_s)(\omega_{o,j}\frac{\omega_{q,p}}{\omega_{o,j}})}e^{i(\phi_j+\delta\phi_p)}e^{-\frac{(t-t_s)}{\tau_j\frac{\tau_{q,p}}{\tau_j}}} \tag{5}$$

where j is an integer and p is an odd integer (same as p in Equation 4). For a given odd p, $A_{q,p}$ is the amplitude of the quantum mode, $\omega_{q,p}$ is the real part of the angular frequency, $\delta\phi_p$ is the relative shift of phase for the new mode, t_s is the relative start time of the new mode, and $\tau_{q,p}$ is the damping time ($1/\omega_{imaginary}$). It is important to note that both $\delta\phi_p$ and $A_{q,p}$ are not well predicted by the model, and depend on *how* the BBH system came together; for this reason, they will be treated as free parameters. The new QNM spectrum, then, will look like a superposition of Equations 5 and 2.

II. PROJECT & METHOD OVERVIEW

This project focuses on testing and employing the quantum modes described by Brustein *et al* [12][13]. The main work of this project is to determine whether the variations (Equation 5) in the GW QNM spectrum are *significantly* detectable by the LIGO network at various signal-to-noise ratios (SNRs) and various BH binary masses. The goal is to find an optimal mass range for detecting these new fluid modes.

First, *without* using quantum deviations, we explore classical GR predictions for the ringdown: what frequencies and damping times are predicted? Next, we will simulate a noiseless signal and fit for ringdown modes, verifying that we can at least recover them. We recover the signal both in `bilby`, which uses Bayesian methods, and with `scipy.optimize` which uses least-squared fitting [15][16].

We move on to looking at the quantum ringdown, exploring the frequency and damping times for various masses and n_{ref}. The modes predicted by Brustein *et al* are derived assuming zero spin. Nevertheless, they argue that including spin will cause a small change in the real part of the frequency. Overall, though, the quantum modes should *still* be lower in frequency and longer lived.

The goal is to see how these new modes compare to GR modes. For our initial analysis, we set the dimensionless spin, $\chi = 0.7$. In general, based on equations 4 and 1 (for $p = 1$), the new quantum mode is expected to be (roughly) lower in frequency and longer lived than the dominant GR quadrupole mode.

Next, we add noise to the quantum ringdown, experimenting with signal-to-noise ratio (SNR) and its relation to BH mass. For this, our parameters are signal amplitude (proxy for SNR), BH mass (in units $M_\odot$), and n_{ref}. We sample mass between $20M_\odot$ and $200M_\odot$, and work with n_{ref} between 3 and 10. We choose to work in this n_{ref} range because it is (1) far from the relativistic modes and (2) prohibitively large n_{ref} will have very low frequencies, undetectable by LIGO and its partners (see Figure 1). We keep $chi = 0.7$ and make a model of *just* the $p = 1$ quantum mode (Equation 5).

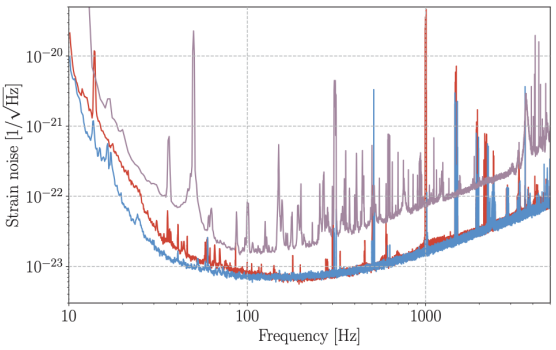

FIG. 1. Noise curves for L1 (blue), H1 (red), and Virgo (purple) [9]. Notice the least noisy band is on the order of 100 Hz.

For our model we assume $p = 1$ because this is the lowest frequency mode; higher values of p (corresponding to higher frequency modes) may begin be to overlap the frequencies of higher order GR modes. For our model we also define the quantum mode's frequency and damping time relative to the (2, 2) mode's. The motivation for this choice is that (1) quadrupolar mode tends to be the loudest and least damped and (2) incorporating higher order modes at this stage adds layers of complexity. We perform our analysis in `bilby` (which works in the frequency domain), beginning at high SNR or high amplitude signals, then moving to lower values until the detection is insignificant. Detection significance, or how well our model is able to match to our simulated signal, is measured by the Bayes factor, which is the likelihood ratio between the quantum model and the null hypothesis (noise). A large Bayes factor (greater than 100) is strong evidence for the quantum model. For ease of sampling, we set the priors on GR mode's parameters (frequency and damping time) to delta functions, and infer the posterior distributions of the quantum frequency and damping time given a uniformly sampled range. From this we should get an optimal mass range for detection for a given n_{ref} value. The optimal mass range *should* differ depending on n_{ref} value.

An important factor to consider is the influence (if there is any) of discontinuities on detection significance, as `bilby` performs its analysis in the frequency domain: sharp transitions in the time domain will result in Gibbs phenomenon [17]. The quantum modes have a delay relative to the GR modes (t_s) and we can define the above analysis starting at t_s, getting rid of the discontinuity in the middle of the waveform, or we can start the analysis from the GR mode's start time (for simplicity, set to 0).

Next, we add the dominant mode, (2, 2), to our model. Here, our goal is to see whether the model with both the quantum and GR mode can be differentiated from a model with *just* the GR mode. Of course, this is a function of mass and SNR, so we follow the same procedure as above. In this analysis, because we have a superposition of a GR and quantum mode, a new parameter is used to describe the fractional amplitude of the quantum mode relative to the GR mode; this is a number between 0 and 1, 0 being no quantum mode, and 1 being a quantum mode with the same amplitude as the GR mode. A realistic fractional amplitude to choose would be small, as a loud quantum mode (with an amplitude comparable to the GR mode) would have already been noticed in GW signals.

III. CURRENT WORK

A. Background Work

As background preparation, I worked through the GW analysis software using the open data workshop tutorials (tutorial Day 1 and tutorial Day 2). From the Day 1 tutorials, I learnt how to use the `gwosc` package for retrieving data and using the `TimeSeries` object in `gwpy` to transform data to the frequency domain (spectrogram, asd, q-transforms, and fft). Also from the Day 1 section I began to use the `pycbc` package. With this package, I was able to create time and frequency domain representations using different approximants; by the end of the tutorial, I was able to see how mass and distance affect the shape

of the resultant waveform, specifically the ringdown.

From the Day 2 tutorials, I learnt how to use the Bayesian parameter estimation package, `bilby`, and the basics of matched filtering with `pycbc`. As I am new to Bayesian statistics and the logistics of sampling methods, I spent some time reading about Bayesian analysis, the `bilby` documentation, and the docs for `dynesty`, which is the preferred nested sampler used by `bilby` [18][19].

B. Simulated Signal Recovery

In `bilby`, I created a general damped-sinusoid model with both plus and cross polarization. The goal was to be sure I could recover my input parameters: amplitude h_0, frequency, and damping time (Figure 2). The main challenge of this was figuring out how to use inputs in `bilby` to speed up the `dynesty` sampling process [19].

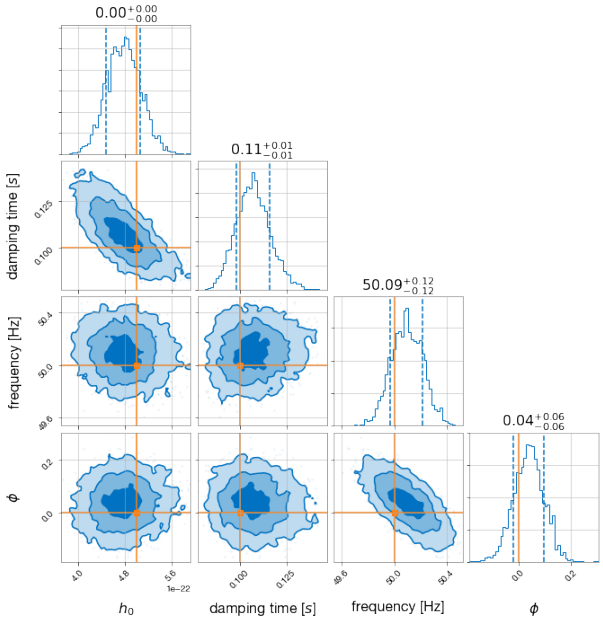

FIG. 2. Recovering input parameters (amplitude h_0, damping time, frequency, and phase ϕ) of single damped sinusoid in `bilby`. The original values of each parameter is marked by the orange lines.

Next, I moved on to create a model that could create a superposition of damped sinusoids (Equation 2). The goal of this task was to create a model of a Kerr BH ringdown for a specific χ, dimensionless spin, and mass. In order to do this, I needed to learn how to use a package to recover QNM. At the beginning, I was experimenting with a package called `pyRing` for BH QNM, but I came across some debugging trouble using it on my computer, so I shifted to the package `qnm`, which recovers the complex-valued frequency for a given mode, (l, m, n) at a given χ [20]. Understanding how to use the `qnm` package, I created a general model of superimposed damped-sinusoids. For simplicity's sake, I kept the amplitude and phase of the modes the same (though this is unphysical, as we would at least expect higher order modes to be smaller in amplitude). I tested the model in `bilby` by creating a superposition of the modes (2, 2, 0), (2, 2, 1), (2, 2, 2), (3, 3, 0) for $\chi = 0.5$ and $M = M_\odot$. I was able to recover the inputted phase, χ, mass, and amplitude (Figure 3).

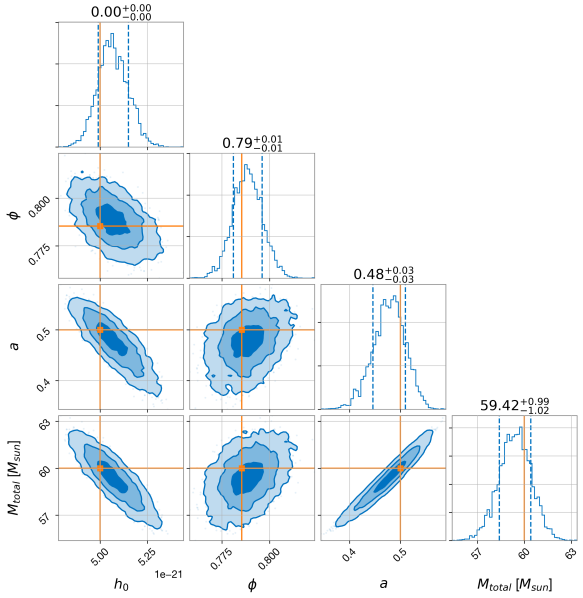

FIG. 3. Recovering input parameters in `bilby` using a superposition of damped sinusoids. The superposition is created from four Kerr QNM modes: (2, 2, 0), (2, 2, 1), (2, 2, 2), (3, 3, 0). Here the sampled parameters are amplitude h_0, M_{total} in units $M_\odot$, dimensionless spin χ, and phase ϕ.

C. GR QNM Visualization & Waveform Optimization

I visualized the effects that different parameters (inclination, mass-ratio q, distance) have on the ringdown for three different models which incorporate higher order modes: NRSur7dq4, SEOBNRv4PHM, and IMRPhenomPv3HM (Figure 4). From this, I saw that NRSur7dq4 (navy) and SEOBNRv4PHM (cyan) have a similar shape, although off by a small phase shift and slightly different in amplitude, at least by eye. IMRPhenomPv3HM (red) appears the most different, off by around a complete cycle.

After looking at the differences in the models, I shifted to looking at NRSur7dq4 in particular, which is able to easily plot modes separately. I saw that $m \neq l$ modes have a lower frequency compared to the dominant (2, 2) mode, and are lower in amplitude (Figure 5).

Next, I worked on seeing if I could recover the expected QNM frequency for a single mode using a damped-sinusoid curve fit (with NRSur7dq4). I chose to work with the fundamental (2, 2) mode, with $M = 44$, $\chi = 0$,

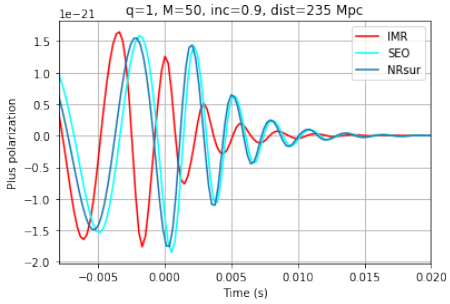

FIG. 4. Ringdown for 3 different models which include higher order modes: NRSur7dq4 (navy), SEOBNRv4PHM (cyan), and IMRPhenomPv3HM (red). Calculated with $M = 50M_{\odot}$, $q = 1$, $inclination = 0.9$, and $distance = 235Mpc$.

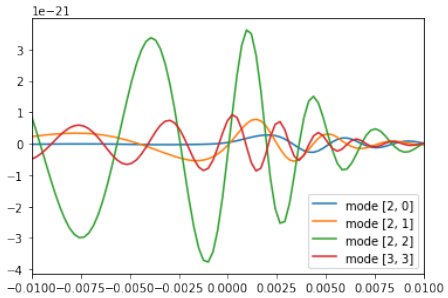

FIG. 5. NRSur7dq4 model: plot of different modes to visualize the relative change of amplitude and frequency. The x-axis represents time (in seconds) and the y-axis is amplitude.

and $q = 1$. From the `qnm` package, this mode should have a frequency of 354 Hz and a decay time of 0.002 seconds. Using `scipy.optimize.curve_fit`, I found that the fit gave me results within the order of the expected QNM: a frequency around 360 Hz and a decay time around 0.002 seconds (Figure 6).

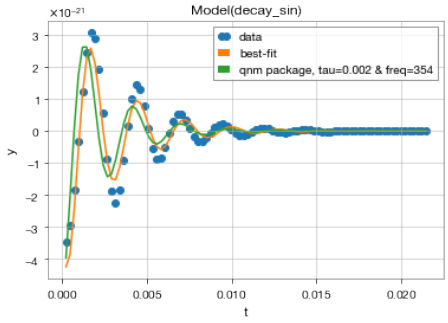

FIG. 6. Fit of NRSur7dq4 model for fundamental (2, 2) mode and $M = 44$, $\chi = 0$, $q = 1$, $distance = 235Mpc$. Here, blue is the NRSur7dq4 model, orange is the found fit (assuming a general damped sinusoid), and green is a plot of the damped sinusoid with ringdown parameters from `qnm`. The fit finds that $tau = 0.002s$ and $f = 260Hz$, while the `qnm` package finds that $f = 254Hz$ and $tau = 0.002s$.

D. GR vs. Quantum Modes

Our choice for n_{ref} and mass influences the frequency and damping time of the quantum modes; spin (χ), for the quantum model, is not considered. Spin and mass influence the frequency and damping time of the classic GR mode. For this reason, we test the effect of (1) spin, (2) mass, and (3) n_{ref} on the complex frequency of various GR and quantum modes in order to see the general differences between the two types of modes (see Figures 7-9 for frequency and Figures 10-13 for damping time). This is important to look at as these factors will influence the detectability of a mode, given that LIGO is most sensitive within a certain band (around 100 Hz, Figure 1). We choose to sample every $10M_{\odot}$ for the sake of speed; the run-time of finer mass (say, every $1M_{\odot}$) takes much longer. Really, rather than discrete points these are smooth curves.

We see that with increasing spin, the GR modes separate from each other, and increase in frequency. Increasing mass, for all modes (GR and quantum), decreases frequency and results in modes being closer together. For small n_{ref}, quantum modes are higher in frequency, but closer to GR modes (see Figures 7-9).

For GR modes, we see that lower spin modes tend to vary the most in damping time with mass. Comparatively, however, the Q modes tend to be longer lived; this tendency increases with mass. Quantum modes with larger n_{ref} have longer damping times (see Figures 10-13).

Although we did not visualize it, the start time (t_s) is also an important thing to consider in this model. The start time of the quantum mode is also delayed with respect to the GR mode (t_s, as noted in Section I, is $1/\omega_{real}$). So, with larger n_{ref}, t_s will be more delayed, and with larger mass, t_s will increase (as frequency tends to *decrease* with increasing mass).

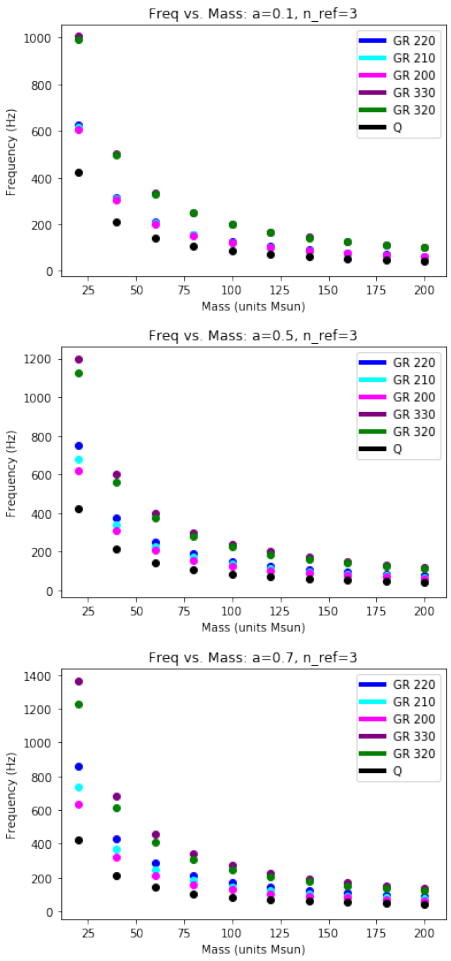

FIG. 7. Plot of frequency vs. mass (in units $M_{\odot}$) for GR modes (from (2,2) to (3,3) and the quantum mode (Q) for $n_{ref} = 3$. GR modes are calculated using `qnm` python package [20]. We see that with increasing χ, the GR modes separate from one another and tend to increase in frequency. For higher mass values, the frequency of *all* modes decreases. The quantum modes are lower in frequency than *all* the plotted GR modes, and the difference in frequency between GR modes and quantum modes decreases with increasing mass.

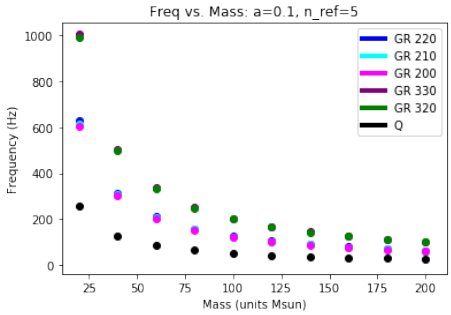

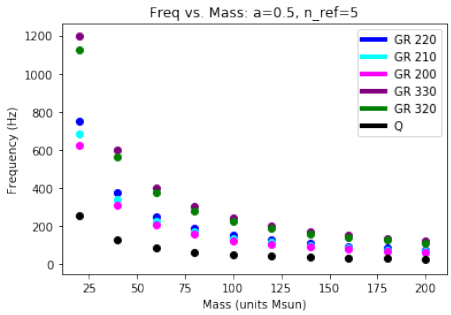

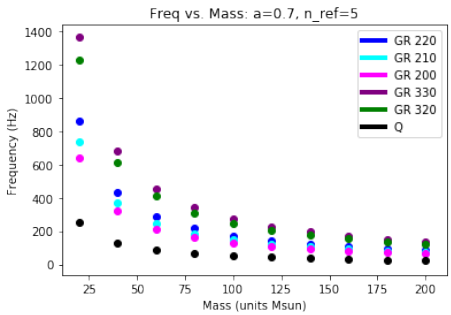

FIG. 8. Plot of frequency vs. mass (in units $M_\odot$) for GR modes (from (2,2) to (3,3) and the quantum mode (Q) for $n_{ref} = 5$. GR modes are calculated using `qnm` python package [20]. We see that with increasing χ, the GR modes separate from one another and tend to increase in frequency. For higher mass values, the frequency of *all* modes decreases. The quantum modes are lower in frequency than *all* the plotted GR modes, and the difference in frequency between GR modes and quantum modes decreases with increasing mass.

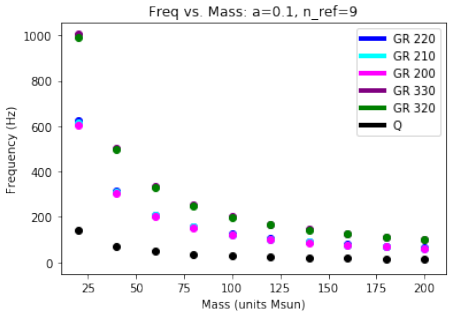

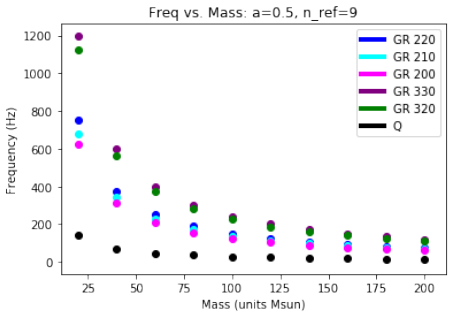

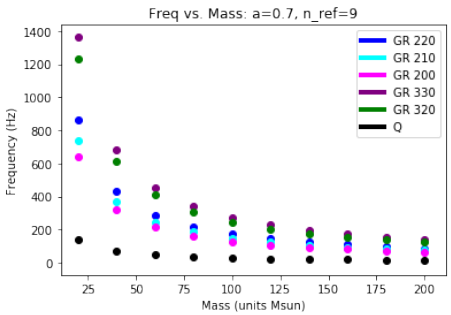

FIG. 9. Plot of frequency vs. mass (in units $M_\odot$) for GR modes (from (2,2) to (3,3) and the quantum mode (Q) for $n_{ref} = 9$. GR modes are calculated using `qnm` python package [20]. We see that with increasing χ, the GR modes separate from one another and tend to increase in frequency. For higher mass values, the frequency of *all* modes decreases. The quantum modes are lower in frequency than *all* the plotted GR modes, and the difference in frequency between GR modes and quantum modes decreases with increasing mass.

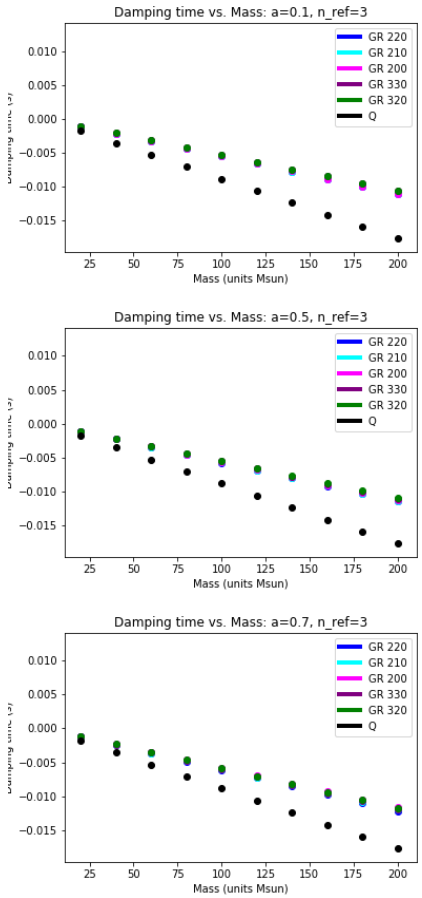

FIG. 10. Plot of damping time vs. mass (in units $M_\odot$) for GR modes (from (2,2) to (3,3) and the quantum mode (Q) for $n_{ref} = 3$. GR modes are calculated using `qnm` python package [20]. We see that with increasing χ, the damping time of GR modes tends to shrink *and* vary less with mass. Overall, the quantum modes are longer lived and have damping times that increase much more with mass.

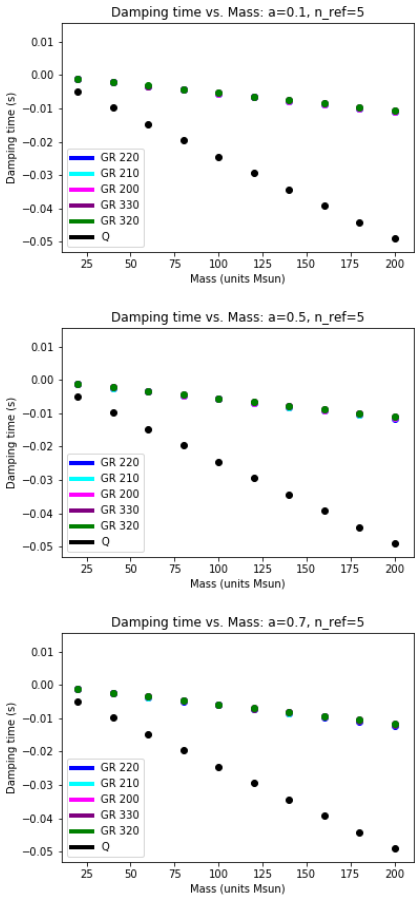

FIG. 11. Plot of damping time vs. mass (in units $M_\odot$) for GR modes (from (2,2) to (3,3) and the quantum mode (Q) for $n_{ref} = 5$. GR modes are calculated using `qnm` python package [20]. We see that with increasing χ, the damping time of GR modes tends to shrink *and* vary less with mass. Overall, the quantum modes are longer lived and have damping times that increase much more with mass.

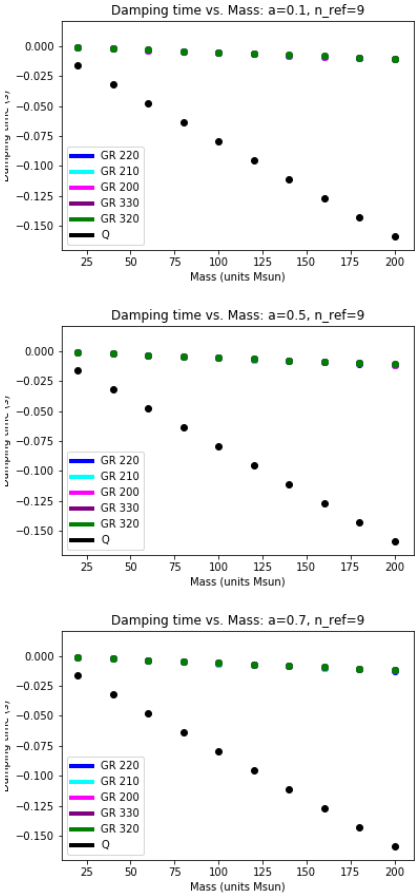

FIG. 12. Plot of damping time vs. mass (in units $M_\odot$) for GR modes (from (2,2) to (3,3) and the quantum mode (Q) for $n_{ref} = 9$. GR modes are calculated using `qnm` python package [20]. We see that with increasing χ, the damping time of GR modes tends to shrink *and* vary less with mass. Overall, the quantum modes are longer lived and have damping times that increase much more with mass.

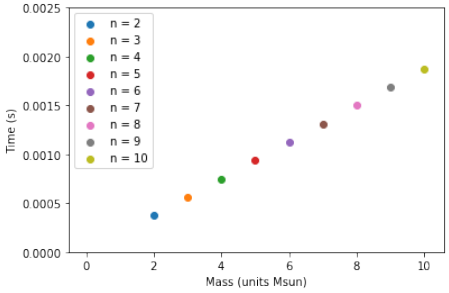

FIG. 13. Plot of n_{ref} value (from 2 to 10) vs. delay time, in seconds, relative to GR mode (which, we will define to start at $t = 0$ for simplicity). for $M = M_\odot$ GR modes are calculated using `qnm` python package [20]. We see that with n_{ref}, the delay time increases. While not plotted, with larger masses, delay times become longer; with smaller masses, delay times become shorter.

E. Recovering Quantum Mode at Different Masses & SNR: including t_s

From Figures 14-17 we see that with increasing n_{ref}, the optimal detection range is shifted towards lower masses. This is expected, as, increasing n_{ref} will result prohibitively low frequencies for high masses (Figure 7-9). In general, we see that very loud signals (high SNR), tend to have the highest log (base 10) Bayes factor, which is unsurprising. Also, the optimal ranges for detection tend to be similar between SNR.

Interestingly, although the exact same parameters and amplitudes were used, the higher values of n_{ref} also tend to have slightly higher log Bayes factors and SNR. Take Figure 14 for $n_{ref} = 3$ and Figure 17 for $n_{ref} = 9$. The highest SNR for $n_{ref} = 3$ falls around 11 (at a Bayes factor near 140). On the other hand, the highest SNR for $n_{ref} = 9$ falls around 20 (at a Bayes factor near 400, which is near double that of $n_{ref} = 3$). This could be the result of choosing a sampling method in `bilby` that is more optimal for larger n_{ref}. It could also be the result of including the t_s discontinuity, which we will explore in the next section.

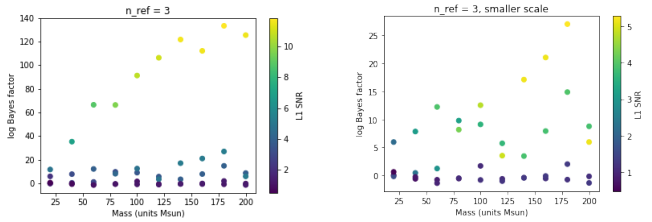

FIG. 14. (Left) For $n_{ref} = 3$, plot of mass (units $M_\odot$) versus log (base 10) at five different peak GW amplitudes: 9×10^{-23}, 1×10^{-22}, 3×10^{-22}, 4×10^{-22}, 9×10^{-22}, resulting in an SNR between 0 and around 11. We see that the highest SNR (and high log Bayes factor) roughly falls around masses between $125M_\odot$ and up. (Right) Same values as the Left plot, but focusing at lower SNR (amplitudes 9×10^{-23}, 1×10^{-22}, 3×10^{-22}, and 4×10^{-22}). Here, the highest SNR falls between $150M_\odot$ and $180M_\odot$, which is a narrower band than in the high SNR case.

We want to see, however, at what (minimum) SNR can parameters be best recovered. To do this, we will compare the parameter recovery at different SNR using `bilby` corner plots of posterior distributions. For simplicity's sake, I will focus on the analysis on the two sides of the n_{ref} spectrum: $n_{ref} = 3$ and $n_{ref} = 9$. I choose to work with the SNR peak values for each; this is $180M_\odot$ for $n_{ref} = 3$ (Figure 18) and $60M_\odot$ for $n_{ref} = 9$ (Figure 19). Overall, it seems as though both n_{ref} are able to recover *at least* to $SNR = 4$ in the case of $n_{ref} = 3$, and $SNR = 7$ in the case of $n_{ref} = 9$.

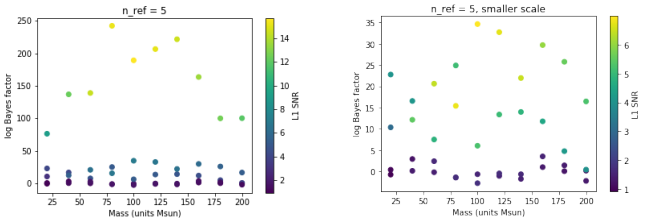

FIG. 15. (Left) For $n_{ref} = 5$, plot of mass (units $M_\odot$) versus log (base 10) at five different peak GW amplitudes: 9×10^{-23}, 1×10^{-22}, 3×10^{-22}, 4×10^{-22} 9×10^{-22}, resulting in an SNR between 0 and around 15. We see that the highest SNR (and high log Bayes factor) roughly falls around masses between $60M_\odot$ to $150M_\odot$. (Right) Same values plotted as the Left plot, but focusing at lower SNR (amplitudes 9×10^{-23}, 1×10^{-22}, 3×10^{-22}, and 4×10^{-22}). Here, the highest SNR and Log Bayes factor falls (roughly) between $60M_\odot$ to $150M_\odot$, which is the same range as the high SNR case.

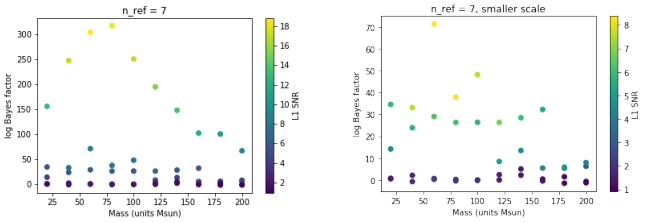

FIG. 16. (Left) For $n_{ref} = 7$, plot of mass (units $M_\odot$) versus log (base 10) at five different peak GW amplitudes: 9×10^{-23}, 1×10^{-22}, 3×10^{-22}, 4×10^{-22} 9×10^{-22}, resulting in an SNR between 0 and around 18. We see that the highest SNR (and high log Bayes factor) roughly falls around masses between $50M_\odot$ to $100M_\odot$. (Right) Same values as the Left plot, but focusing at lower SNR (amplitudes 9×10^{-23}, 1×10^{-22}, 3×10^{-22}, and 4×10^{-22}). Here, the highest SNR and Log Bayes factor falls (roughly) between $50M_\odot$ to $100M_\odot$, which is close to the same range as the high SNR case.

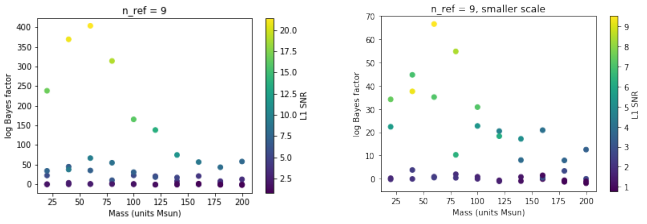

FIG. 17. (Left) For $n_{ref} = 9$, plot of mass (units $M_\odot$) versus log (base 10) at five different peak GW amplitudes: 9×10^{-23}, 1×10^{-22}, 3×10^{-22}, 4×10^{-22}, 9×10^{-22}, resulting in an SNR between around 0 and 20. We see that the highest SNR (and high log Bayes factor) roughly falls around masses between $40M_\odot$ to $80M_\odot$. (Right) Same values as the Left plot, but focusing at lower SNR (amplitudes 9×10^{-23}, 1×10^{-22}, 3×10^{-22}, and 4×10^{-22}). Here, the highest SNR and Log Bayes factor falls (roughly) between $40M_\odot$ to $80M_\odot$, which is close to the same range as the high SNR case.

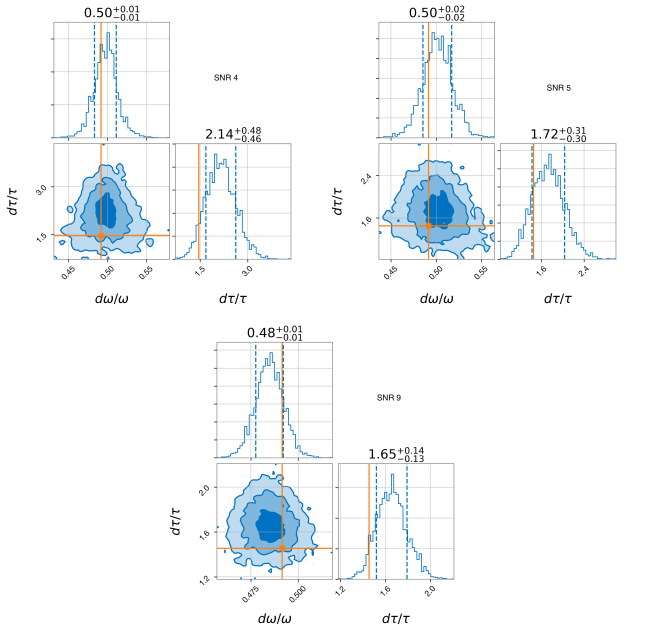

FIG. 18. Posterior distribution corner plots for $n_{ref} = 3$, $M = 180M_\odot$ and SNR 4, 5, and 9 (as labeled). The input $\delta\omega/\omega = 0.49155$ while the input $\delta\tau/\tau = 1.45$ (again, these are in reference to the dominant (2, 2) mode). We see that, while out error bars sometimes do not include our inputted value, with increasing SNR, the peak nears our input, especially with regard to $\delta\tau/\tau = 1.45$.

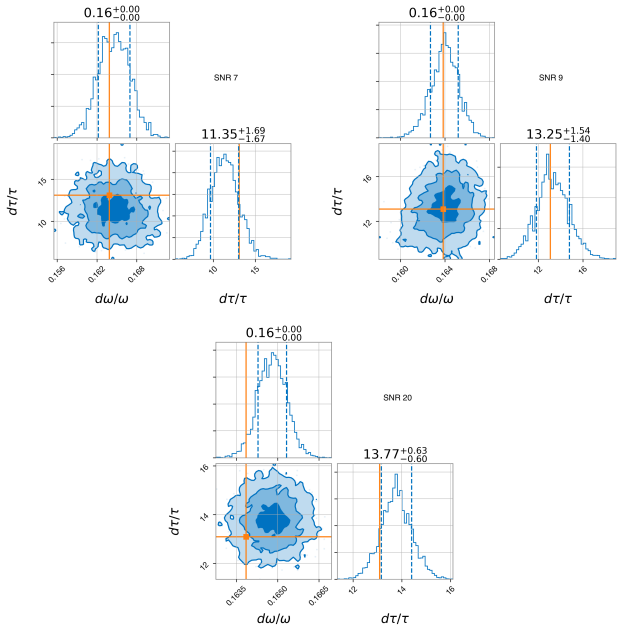

FIG. 19. Posterior distribution corner plots for $n_{ref} = 9$, $M = 60M_\odot$, and SNR 7, 9, and 20 (as labeled). The input $\delta\omega/\omega = 0.16$ while the input $\delta\tau/\tau = 13.08$ (again, these are in reference to the dominant (2, 2) mode). We see that, while our error bars sometimes do not include our inputted value, with increasing SNR, the peak is near to input, especially with regard to $\delta\tau/\tau = 1.45$.

F. Recovering Quantum Mode at Different Masses & SNR: not including t_s

The bad implementation of t_s, which causes a discontinuity in the waveform, can affect analysis in the frequency plane and is unphysical. This is important to look at for double checking the analysis above and before moving onto a superposition of modes.

We explore this to understand the discontinuity's effects on (1) SNR and (2) parameter recovery. For speed of analysis we focus on high SNR, as presumably, the optimal mass range will not vary much (as we found above). Comparing Figures 7 - 9 (which include t_s with Figures 20 - 23 (which *do not* include t_s) we see that both the peaks are sharper (and shifted) when t_s is not included, making the optimal mass range more narrow. The highest SNR does not really vary between the two methods. Interestingly, we again see the same pattern: higher values of n_{ref} tend to have slightly higher log Bayes factors and SNR.

Next, we move on to looking at parameter recovery (Figures 24 and 25). We will again explore the two extremes for n_{ref} – 3 and 9 – and pick the mass at which SNR peaks. In the case of $n_{ref} = 3$ this is $140M_\odot$ (which is shifted from before, see Figure 7). For $n_{ref} = 9$ it is the same as Figure 9, at $60M_\odot$. Overall, there seems to be no stark difference between using $t_s = 0$ and including t_s with regard to parameter recovery. For instance, if we compare parameter recovery of n_{ref} at SNR 9 (Figures 19 and 25) while peaks are slightly different, error bounds are near equivalent.

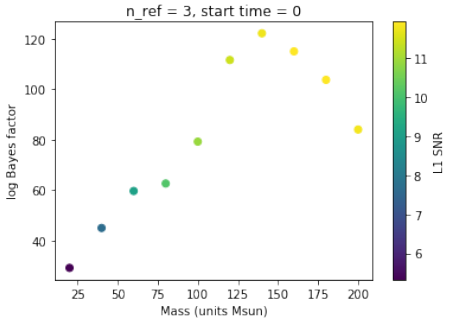

FIG. 20. For $n_{ref} = 3$ starting the waveform at $t_s = 0$, plot of mass (units $M_\odot$) versus log (base 10) amplitude 9×10^{-22}, resulting in a highest SNR of around 12 around the mass of $160M_\odot$.

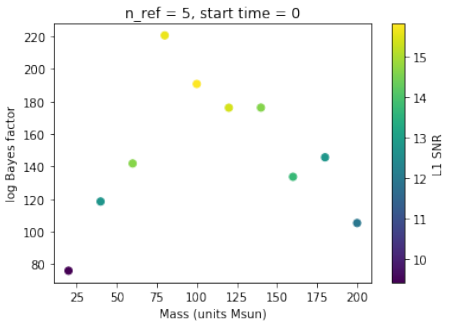

FIG. 21. For $n_{ref} = 5$ starting the waveform at $t_s = 0$, plot of mass (units $M_\odot$) versus log (base 10) amplitude 9×10^{-22}, resulting in a highest SNR of around 15 around the mass of $80M_\odot$.

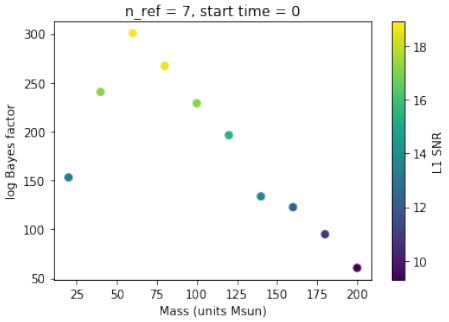

FIG. 22. For $n_{ref} = 7$ starting the waveform at $t_s = 0$, plot of mass (units $M_\odot$) versus log (base 10) amplitude 9×10^{-22}, resulting in a highest SNR of around 18 around the mass of $60M_\odot$.

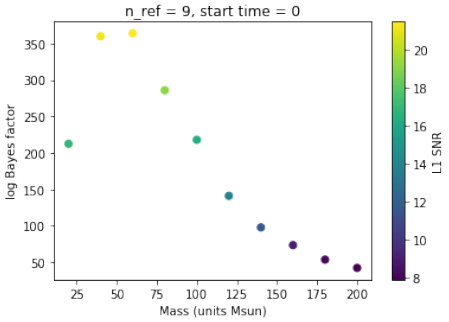

FIG. 23. For $n_{ref} = 9$ starting the waveform at $t_s = 0$, plot of mass (units $M_\odot$) versus log (base 10) amplitude 9×10^{-22}, resulting in a highest SNR of around 20 around the mass of $60M_\odot$.

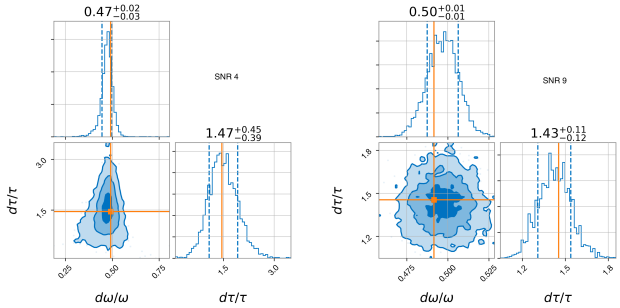

FIG. 24. Using $t_s = 0$, posterior distribution corner plots for $n_{ref} = 9$, $M = 60M_\odot$, and SNR 4 and 9 (as labeled). The input $\delta\omega/\omega = 0.49155$ while the input $\delta\tau/\tau = 1.45$ (again, these are in reference to the dominant (2, 2) mode). We see that, while our error bars sometimes do not include our inputted value, with increasing SNR, the peak nears our input, especially with regard to $\delta\tau/\tau = 1.45$.

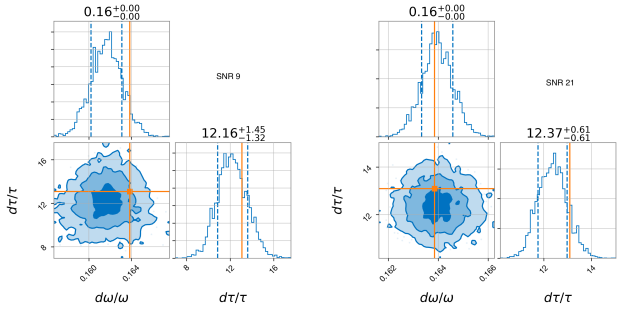

FIG. 25. Using $t_s = 0$, posterior distribution corner plots for $n_{ref} = 9$, $M = 60M_\odot$, and SNR 9 and 21 (as labeled). The input $\delta\omega/\omega = 0.16$ while the input $\delta\tau/\tau = 13.08$ (again, these are in reference to the dominant (2, 2) mode). We see that, while our error bars sometimes do not include our inputted value, with increasing SNR, the peak is near to input, especially with regard to $\delta\tau/\tau = 1.45$.

IV. CHALLENGES & RESEARCH GOALS MOVING FORWARD

One of the main challenges has been running the sampler, as sampling a range of masses can take anywhere from thirty minutes to three hours (depending on the model). This may speed up given that I have a better idea of what masses work best for each n_{ref}.

Another thing that I am working to understand is why the higher values of n_{ref} tend to have slightly higher log Bayes factors and SNRs. Since it does not seem to be a result of t_s, I am thinking that it might be because of how I defined the prior sampling in `bilby`. A more robust way to go about analysis may be to run the analysis above at different sampler settings, and see differences. This, however, will be time consuming, so exploring this may need to be put on the back burner.

Moving forward, I am going to add the dominant mode to the model, and see if the optimal mass ranges changes. I would expect that the mass range *would* change, as the game would now be to detect the GR mode *and* the quantum mode. I will define the amplitude of the quantum mode relative to the GR mode (some number between 0 and 1); realistically, this number is small.

After this, time permitting, I would like explore the likelihood ratio of the quantum model vs. the GR model; this will be a function of SNR/mass. In other words, if we inject quantum mode in the signal, will the more complicated model (the one that include the quantum mode) be preferred over the GR (more simple) model?

[1] T. Moore, *A General Relativity Workbook* (University Science Books, 2012).

[2] L. S. Collaboration and *et al*, Advanced ligo, arXiv (2015).

[3] F. Acernese and *et al*, Advanced virgo: a second-generation interferometric gravitational wave detector, arXiv (2015).

[4] B. P. Abbott and *et al*, Observation of gravitation waves from a binary black hole merger, Phys. Rev. Letters **116** (2016).

[5] V. C. Emanuele Berti and A. O. Starinets, Quasinormal modes of black holes and black branes, arXiv (2009).

[6] R. A. Konoplya and A. Zhidenko, Quasinormal modes of black holes: from astrophysics to string theory, arXiv (2011).

[7] LIGO and VIRGO, Gw190412: Observation of a binary-black-hole coalescence with asymmetric masses, arXiv (2020).

[8] Lorentzian function: Wolfram mathworld, `https://mathworld.wolfram.com/LorentzianFunction.html`.

[9] B. P. Abbott and *et al*, Gwtc-1: A gravitational-wave transient catalog of compact binary mergers observed by ligo and virgo during the first and second observing runs, Phys. Rev.X **9** (2019).

[10] R. Abbott and *et al*, Gw190814: Gravitational waves from the coalescence of a 23 solar mass black hole with a 2.6 solar mass compact object, arXiv (2020).

[11] R. Brustein and A. Medved, Non-singular black holes interiors need physics beyond the standard model, Progress of Physics **67** (2019).

[12] R. Brustein and Y. Sherf, Emission channels from perturbed quantum black holes, Phys. Rev. D **100** (2019).

[13] A. M. Ram Brustein and K. Yagi, When black holes collide: Probing the interior composition by the spectrum of ringdown modes and emitted gravitational waves, arXiv (2017).

[14] A. Z. . D. Robbins, *String Theory for Dummies* (Wiley Publishing, 2010).

[15] Bilby documentation, `https://lscsoft.docs.ligo.org/bilby/index.html`.

[16] Scipy docs, `https://docs.scipy.org/doc/scipy/reference/tutorial/optimize.html`.

[17] Gibbs phenomenon, `https://mathworld.wolfram.com/GibbsPhenomenon.html`.

[18] G. Ashton and *et al*, Bilby: A user-friendly bayesian inference library for gravitational-wave astronomy, arXiv (2018).

[19] Dynamic nested sampling with dynesty, `https://dynesty.readthedocs.io/en/latest/dynamic.html`.

[20] `qnm` documentation, `https://qnm.readthedocs.io/en/latest/`.